Geomech. Geophys. Geo-energ. Geo-resour. (2023) 9:124
https://doi.org/10.1007/s40948-023-00661-w

RESEARCH

Weakening of mechanical parameters of ion-absorbed rare-earth ores subjected to leaching

Hao Wang · Xiaojun Wang · Gang Li · Huachang Ye · Cheng Zhang · Lingbo Zhou

Received: 13 July 2023 / Accepted: 19 September 2023

Abstract Ion-adsorbed rare-earth ores are mined using in-situ leaching, and their mechanical properties significantly affect the efficient and safe recovery of rare earth elements. However, the mechanism of the change in the mechanical properties of the ore body due to the physicochemical processes caused by leaching remains unclear. To explore the strength evolution characteristics of the ore body during the leaching process, unconsolidated undrained triaxial tests were conducted to confirm how the stress–strain curve and shear strength of rare-earth samples change during leaching. Magnetic resonance imaging and T_2 spectral characterizations were obtained by using nuclear magnetic resonance technology to measure the interior pore structure of samples during leaching. A scanning electron microscope equipped with an energy dispersive spectrometer was used to investigate the morphology evolution and the composition changes of the internal micro-area of the samples, to demonstrate the correlation between the microstructural change and the macroscopic mechanical properties. The results show that when a 2% ammonium sulfate solution is employed for mineral leaching, the effective leaching duration is 0–3 h. During this time, ion exchange occurs along the direction of solution seepage, resulting in the dispersion and migration of fine particles from the top to the bottom of the sample, which further triggers a change in the sample's pore structure and pore size. In addition, the local loss of fine particles resulted in a reduced bond strength between minerals, forming an unstable soil structure with a loose upper part and a dense lower part, which is macroscopically expressed as a declining shear strength parameter of the rare-earth sample.

H. Wang · X. Wang (✉) · G. Li
School of Resources and Environment Engineering, Jiangxi University of Science and Technology, Ganzhou 341000, China
e-mail: wangxiaojun@jxust.edu.cn

X. Wang
School of Emergency Management and Safety Engineering, Jiangxi University of Science and Technology, Ganzhou 341000, China

H. Ye
Pingyuan County Huaqi Rare Earths Industry Co., Ltd, Meizhou 514000, Guangdong, China

C. Zhang
Ganzhou Rare Earth Mining Co., Ltd, China Rare Earth Group Co., Ltd, Ganzhou 341000, China

L. Zhou (✉)
Ganjiang Innovation Academy, Chinese Academy of Sciences, Ganzhou 341000, China
e-mail: lbzhou21@gia.cas.cn

Published online: 29 September 2023

Graphical abstract

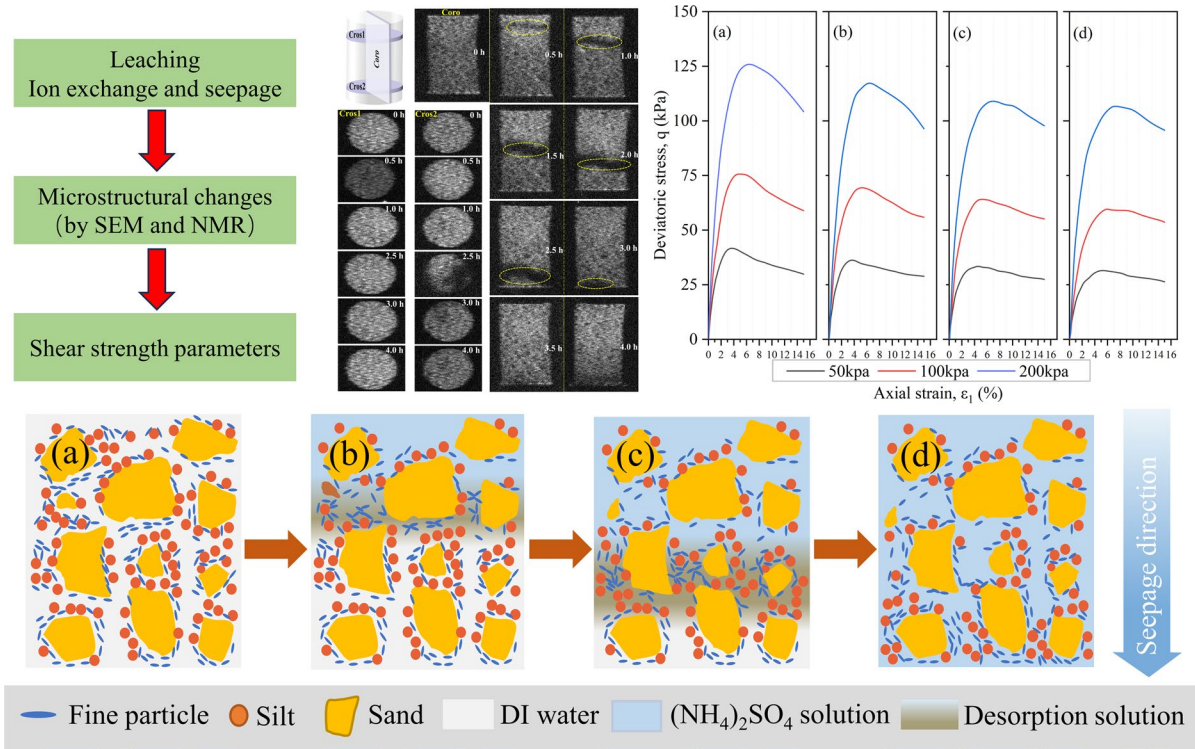

Article highlights

- The effect of leaching on the microstructural characteristics of ion-adsorbed rare-earth ore samples is investigated.
- The change in microstructural characteristics is highlighted by SEM and NMR.
- The mechanical and microstructural properties present a good mutual correspondence.
- The mechanism of shear strength parameters weakening in leaching is discussed.

Keywords Ion-absorbed rare-earth ores · UU triaxial · Ion exchange · Mechanical properties · Microstructure

1 Introduction

Ion-absorbed rare-earth ores represent a unique mineral resource rich in medium-heavy rare-earth elements. They have been successively discovered in different geographic regions worldwide, being abundant in southern China (Borst et al. 2020; Dushyantha et al. 2020; Stockdale and Banwart 2021). After long-term weathering of rare-earth-bearing granite or volcanic rocks, ion-absorbed rare-earth ores reaches the final state of degradation conducting to a soil form enriched with rare-earth elements (Deng et al. 2019; Fu et al. 2019; Yang et al. 2019). In this type of deposit, the occurrence of rare-earth elements involves their adsorption onto clay minerals in the weathering layer, primarily in the form of hydrated cations or hydroxy hydrous cations. Thus, an electrolyte solution of a certain concentration can easily desorb the rare-earth ions by ion exchange (Moldoveanu and Papangelakis 2012, 2013; Yang et al. 2018). Three generations of mining techniques have been used on ion-absorbed rare-earth ores: vat leaching, heap leaching, and in-situ leaching (Yang et al. 2013; Zhang et al. 2016). Currently, in-situ leaching is primarily applied to extract rare-earth resources, and leaching agents have evolved from sodium chloride to

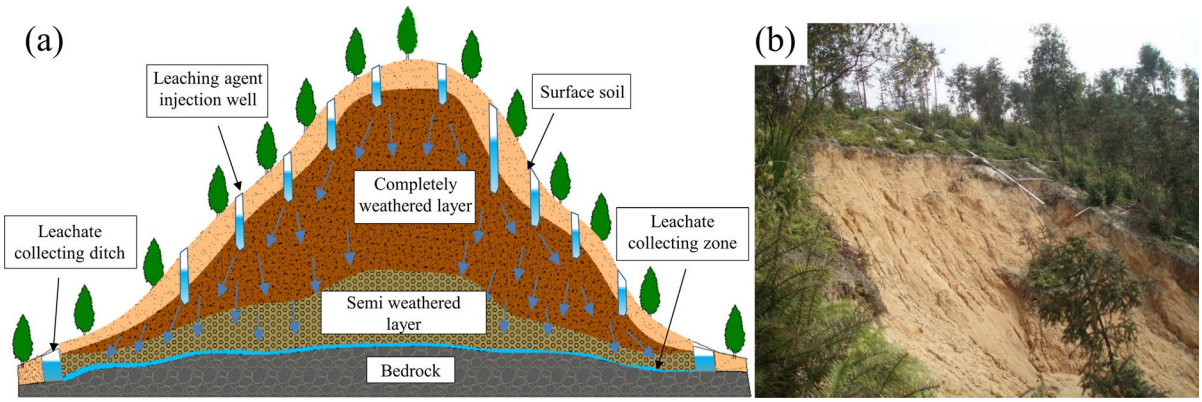

Fig. 1 Landslide caused by in-situ leaching **a** Diagrammatic representation of in-situ leaching; **b** scene of ore body landslide

ammonium sulfate solution, which is commonly used nowadays (Huang et al. 2015; Zhang et al. 2016; Nie et al. 2020). The leaching procedure assumes that the rare-earth ore body is continually injected with a significant volume of electrolyte solution, during which cations from the electrolyte solution replace rare-earth ions; then, the desorbed rare-earth ions in the solution are seeped out from one side of the collecting ditch and pooled in a collecting reservoir to form rare-earth-enriched liquor, as shown in Fig. 1a. Compared with the previous two generations of leaching processes, an in-situ leaching process is favorable due to the shortened project time, lower construction cost, the steady high recovery efficiency of rare-earth elements, and vegetation protection (Huang et al. 2015). According to the rare-earth mine landslide survey data from the Ganzhou area, China possesses the highest number of sites for mineral discovery and represents the main producing area of rare-earth elements; however, 719 of the 890 landslide accidents occurred during in-situ leaching, dominated by shallow landslides (Chen et al. 2021). The survey results indicate that continuous agent injection changes the physical and mechanical properties of rare-earth ores, degrading or depriving their values in engineering applications (Yang et al. 2013; Zhang et al. 2016). For the safe and effective extraction of rare-earth resources, it is crucial to understand the mechanical behavior and mechanism of the rare-earth ore body throughout the leaching process.

As a weathered soil, ion-absorbed rare-earth ores exhibits a loose texture, comprising sand, silt, and clay, with a notable presence of fine particles measuring less than 75 μm in the weathered layer (Chen et al. 2020). Consequently, variations in both physical and chemical conditions possess the potential to impact the shear strength of the soil (Guo et al. 2022). The research community initially directed its attention towards investigating changes in water content resulting from fluid injection (Tang et al. 2000; Wang et al. 2017; Hong et al. 2019). This process involves transitioning the ore body from an unsaturated to a saturated state, during which an increase in water content induces a reduction in effective stress, thereby establishing it as a pivotal factor influencing landslide occurrences. Nevertheless, geological hazard statistics from the Ganzhou area demonstrate that the risk of landslides during leaching surpasses the one associated with the episodes of intense rainfall (Peng et al. 2017). This discrepancy suggests that the increment in water content alone cannot adequately elucidate the phenomenon of landslides. To address this knowledge gap, numerous endeavors have been undertaken to comprehensively evaluate the influence of diverse parameters, encompassing soil properties (such as soil texture, grain size, and pore structure) (Salgado et al. 2000; Li et al. 2019; Sadeghi et al. 2019; Gong et al. 2022), and fluid properties (including pH, solution type, and concentration) (Gratchev and Towhata 2013; Lei et al. 2020; Bai et al. 2023; Yang et al. 2023), on the mechanical properties. Wang and Li (2022) conducted in situ shear tests, revealing a strong correlation between the shear strength of in-situ rare-earth ore samples and the particle size grading as well as the void ratio. Yin et al. (2018) manipulated rare-earth samples with specific

particle size gradations and transformed them into specimens with varying void ratios for direct shear tests. The results demonstrated that as the void ratio decreased, the shear strength increased. This can be attributed to a smaller void ratio facilitating a larger contact area between particles, thereby enhancing particle interlock strength. Moreover, when the coarse particle skeleton of the soil remains constant, a reduction in fine particle content results in fewer interparticle contacts and diminished shear resistance, consequently impacting the overall shear strength (Chen et al. 2019). Liu et al. (2020a) conducted direct shear tests on specimens with different particle distributions obtained through sieving. The findings indicated that smaller particles possessed a larger specific surface area, which led to the formation of a thicker bound water film and a smaller particle contact surface. Consequently, cohesion increased, friction weakened, and shear strength decreased. Conversely, coarse particles exhibited the opposite behavior. Peng et al. (2022) demonstrated that alterations in ammonium sulfate concentration exert an influence on particle size, consequently impacting shear strength parameters. In summary, previous research has mainly explored how macroscopic physical and chemical conditions affect the shear strength of rare-earth ores, with limited attention given to understanding the underlying mechanisms causing the mechanical properties of rare-earth ores to deteriorate during leaching.

The microstructure of soil plays a pivotal role in governing the behavior of the soil, whether it is in its original or modified state, by defining the arrangement of its constituent particles and pores (Xiao et al. 2022; Yuan and Fan 2022). The understanding of macroscopic soil behavior and engineering properties, including permeability and mechanical properties, can be elucidated through microstructure experiments (Li et al. 2019; Lei et al. 2020; Xu et al. 2021). Traditionally, studies have relied on the initial microstructure established during soil preparation to assess the subsequent mechanical behavior (Yin et al. 2018; Liu, et al. 2020a). Nonetheless, it should be acknowledged that any physical and chemical modifications occurring within a soil sample possess the potential to induce alterations in its microstructure. During the in-situ leaching process, a series of physical and chemical processes, including the ion-exchange reaction and soil erosion by water flow, inevitably happen when the electrolyte flows through the rare-earth ore body. Consequently, these processes induce notable changes in the properties of the ore body, encompassing alterations in surface potential, particle size, density, and pore structure (Chen et al. 2020; Liu et al. 2020b; Guo et al. 2021; Zhou et al. 2021; Luo et al. 2022), thereby bringing about a transformation in the ore body's original microstructure. These findings demonstrate that relying solely on the initial microstructure is insufficient to fully comprehend the mechanical behavior. Moreover, it is worth noting that the majority of microstructure tests have primarily focused on characterizing the permeability properties of rare-earth ore bodies (Liu et al. 2020b; Wang et al. 2020; Yin et al. 2021; Zhang et al. 2021; Zhou et al. 2021; Luo et al. 2022), with less emphasis on investigating their mechanical properties. Hence, a comparative analysis was conducted on the microstructure of a series of ore samples during the leaching process, to investigate the corresponding changes in their mechanical properties.

This study aims to investigate the mechanical property changes of ore samples during the leaching process and unravel their underlying mechanisms through microstructure characterization. A systematic approach, including column leaching tests, triaxial shear tests, SEM and NMR analysis, was employed. The results provide insights into the microstructural changes during leaching, their correlation with the shear strength parameters of the ore body and the mechanisms behind its weakening, and are expected to provide a scientific basis for future leaching process optimization and risk prevention.

2 Materials and methods

2.1 Soil samples and physical properties

The soil samples used in this experiment were obtained from a ion-adsorption rare-earth mine located in Longnan, Ganzhou City, Jiangxi Province. According to the Chinese standard of geotechnical test GB/T 50123–2019 (2019), the physical parameters of undisturbed rare-earth ore samples, including particle size distribution, natural bulk density (ρ), specific gravity (ω), and natural soil moisture content (θ), were determined and are presented in Table 1.

Table 1 Physical parameters of Longnan rare-earth ore sample

Parameters	ρ g·cm^{-3}	θ %	ω	Distribution in particle size /%						
				≥5 mm	5–1 mm	0.5–1 mm	0.1–0.5 mm	0.075–0.1 mm	0.075–0.005 mm	<0.005 mm
Value	1.75	13	2.68	2.51	17.28	16.36	39.06	9.82	10.61	4.36

Table 2 The main chemical composition of rare-earth ore sample (mass fraction %)

Element	RE_2O_3	Na_2O	MgO	Al_2O_3	SiO_2	SO_3	K_2O	CaO	Fe_2O_3
Content	0.07	0.09	0.04	30.62	61.55	0.03	5.53	0.04	1.61

Table 3 The partitioning of rare earths (mass fraction %)

Element	La_2O_3	CeO_2	Pr_6O_{11}	Nd_2O_3	Sm_2O_3	Eu_2O_3	Gd_2O_3	Tb_4O_7
Content	7.06	14.83	2.47	10.22	4.75	0.11	5.50	1.01
Element	Dy_2O_3	Ho_2O_3	Er_2O_3	Tm_2O_3	Yb_2O_3	Lu_2O_3	Y_2O_3	
Content	6.23	1.26	3.73	0.61	4.29	0.64	37.30	

In addition, Table 2 shows the chemical composition of the ore sample as measured by X-ray Fluorescence (Axios max, PANalytical B.V.), it can be observed that SiO_2 (61.55%), Al_2O_3 (30.63%) have the highest contents among the chemical components, and the other chemical components with high contents are K_2O (5.53%). The rare-earth content in Table 2 and its partitioning (see Table 3) were determined by inductively coupled plasma mass spectrometry (ICP-MS) (Agilent 8800, Agilent). The rare-earth ore was medium yttrium, containing 0.07% rare earths.

2.2 Ion-exchange analysis

The leaching process can be described as the desorption process or ion-exchange process of rare earths (Xiao 2015; Moldoveanu and Papangelakis 2013). With the leaching solution injected into the orebody, seepage occurred under the action of gravity, only the rare earths in the exchangeable state (which are physically adsorbed on the surface of clay minerals mainly in the form of trivalent cations) can be exchanged from the rare-earth ore by cations (NH_4^+, Na^+, Mg^{2+}, Al^{3+} etc.) in the solution (Zhang et al. 1995; Chi et al. 2005; Moldoveanu and Papangelakis 2012). Meanwhile, other exchangeable impurity metal ions also can be released into the solution by ion exchange, albeit at extremely low concentrations (Wang et al. 2023). The main clay minerals in rare-earth ore were aluminosilicate, which can be described as $[Al_2Si_2O_5(OH)_4]_m{\cdot}xRE^{3+}$ for kaolinite, $[Al(OH)_6Si_2O_5(OH)_3]_m{\cdot}xRE^{3+}$ for halloysite and $[KAl_2[AlSi_3O_{10}](OH)_2]_m{\cdot}xRE^{3+}$ for muscovite. The main chemical reaction equation in the column leaching process generally follows the equivalent exchange of ions, as shown in Eqs. (1)–(3) (Tian et al. 2010; Guo et al. 2021).

$$[Al_2Si_2O_5(OH)_4]_m \cdot xRE^{3+}_{(s)} + 3x/yM^{y+}_{(aq)} \rightarrow [Al_2Si_2O_5(OH)_4]m \cdot 3x/y(M^{y+})_{(s)} + xRE^{3+}_{(aq)} \quad (1)$$

$$[Al(OH)_6Si_2O_5(OH)_3]_m \cdot xRE^{3+}_{(s)} + 3x/yM^{y+}_{(aq)} \rightarrow [Al(OH)_6Si_2O_5(OH)_3]m \cdot 3x/y(M^{y+})_{(s)} + xRE^{3+}_{(aq)} \quad (2)$$

$$[KAl_2(AlSi_3O_{10})(OH)_2]_m \cdot xRE^{3+}_{(s)} + 3x/yM^{y+}_{(aq)} \rightarrow [KAl_2(AlSi_3O_{10})(OH)_2]m \cdot 3x/y(M^{y+})_{(s)} + xRE^{3+}_{(aq)} \quad (3)$$

where RE^{3+} is rare-earth ions; M^{y+} is cations with relatively active chemical properties, such as Na^+, NH_4^+, Mg^{2+}, Ca^{2+}, Al^{3+}.

2.3 Experimental process

Undisturbed ore soils have a loose structure and poor cohesion, and are not conducive to intact preservation during transportation; therefore, in order to prepare standard test samples, the collected soil samples were remolded and used in subsequent tests. The strength-weakening mechanism of the ion-absorbed rare-earth ore body during leaching was investigated using various experimental methods, as shown in Fig. 2. Three groups of tests were designed as the UU triaxial test, and a confining pressure of 50, 100, and 200 kPa was used for each group of tests, respectively, to adapt to the stress state of the shallow ore body.

(1) Sample preparation: a wet compaction method was used to prepare the remodeled soil samples to facilitate the control of the physical parameters of the specimens in line with those of the undisturbed soil. The compacted soil was prepared using the following procedure suggested by (Aiban et al. 2006; Xu et al. 2021): first, drying the collected soil samples in an oven at 105 °C for 10 h. Secondly, mixing the dried soil samples with deionized water (DI water) to reach a natural soil moisture content of approximately 13% (Table 1), subsequently placing them in a sealed bag for 24 h to achieve water homogeneity. Finally, a known amount of pre-treated soil samples was compacted in a mold using membrane barrel and compactor to obtain remolded soil samples with target density of 1.75 $g{\cdot}cm^{-3}$. To adapt to the subsequent column leaching and NMR tests on the samples, the samples were designed with a unified height of 60 mm and diameter of 39.1 mm. The sample preparation instrument and the remolded rare-earth ore sample are shown in Fig. 2a.

(2) Column leaching test: the column leaching device is shown in Fig. 2b. Before liquid injection, two layers of filter paper were laid on the upper end of the sample as a buffer to protect the sample against damage. The lower end of the sample was padded with a metal mesh plate with a mesh diameter of 0.1 mm, allowing water and fine particles to flow out of the sample (Chitravel et al. 2021). Effluent leachate was collected in the measuring cylinder below. The solution flew into the rubber membrane through the upper guide tube, and the leaching solution retained the same flow rate. A 2% $(NH_4)_2SO_4$ solution was used in this test for ore leaching, and a series of remolded rare-earth ore samples with almost the same initial pore structure were selected for the column leaching test. It is important to notice that before being leached with the 2% $(NH_4)_2SO_4$ solution, all samples were saturated for 24 h with DI water from top to bottom to distinguish the seepage from the ion exchange function. During leaching with the 2% $(NH_4)_2SO_4$ solution, leachate was collected once every 0.5 h. The concentrations of the RE^{3+} ions and NH_4^+ ions in the leachate were detected using the EDTA titration and UV-5100 spectrophotometer (Shanghai Metash Instruments Co., Ltd), respectively (Fig. 2c). Each leaching of the sample for 0.5 h was defined as one leaching recycle, and then the sample was taken out for the NMR test. After the test, the sample was collected and dried, and then the content of rare-earth oxides (REO) was tested by ICP-MS (see Fig. 2d).

(3) NMR test: an NMR analyzer (MesoMR23-060H, Suzhou Niumai Analytical Instrument Corporation) was used for obtaining MRI images and T_2 spectrum of the sample, as shown in Fig. 2e. Before the test, the permanent magnet inside the test instrument was adjusted to stabilize at 32 ± 0.1 °C to ensure the accuracy of test imaging. When the leaching started, the sample was taken out every 0.5 h for the pore structure test until the end of the test.

(4) UU triaxial test: a YSZZ-1 triaxial test instrument (Jiangsu Yongsheng Fluid Technology Corporation), Fig. 2f, was used for the mechanical test. According to the early-stage ore leaching test, a group of samples taken out after 0, 1, 2 or 3 h of leaching were tested, and three different confining pressures, σ_3, that is, 50, 100, and 200 kPa, respectively, were defined for the strength test at each period. The test was conducted at an axial shear rate of 0.5 $mm{\cdot}min^{-1}$.

(5) SEM and EDS tests: remolded rare-earth samples made in the same batch were additionally selected for the parallel column leaching test.

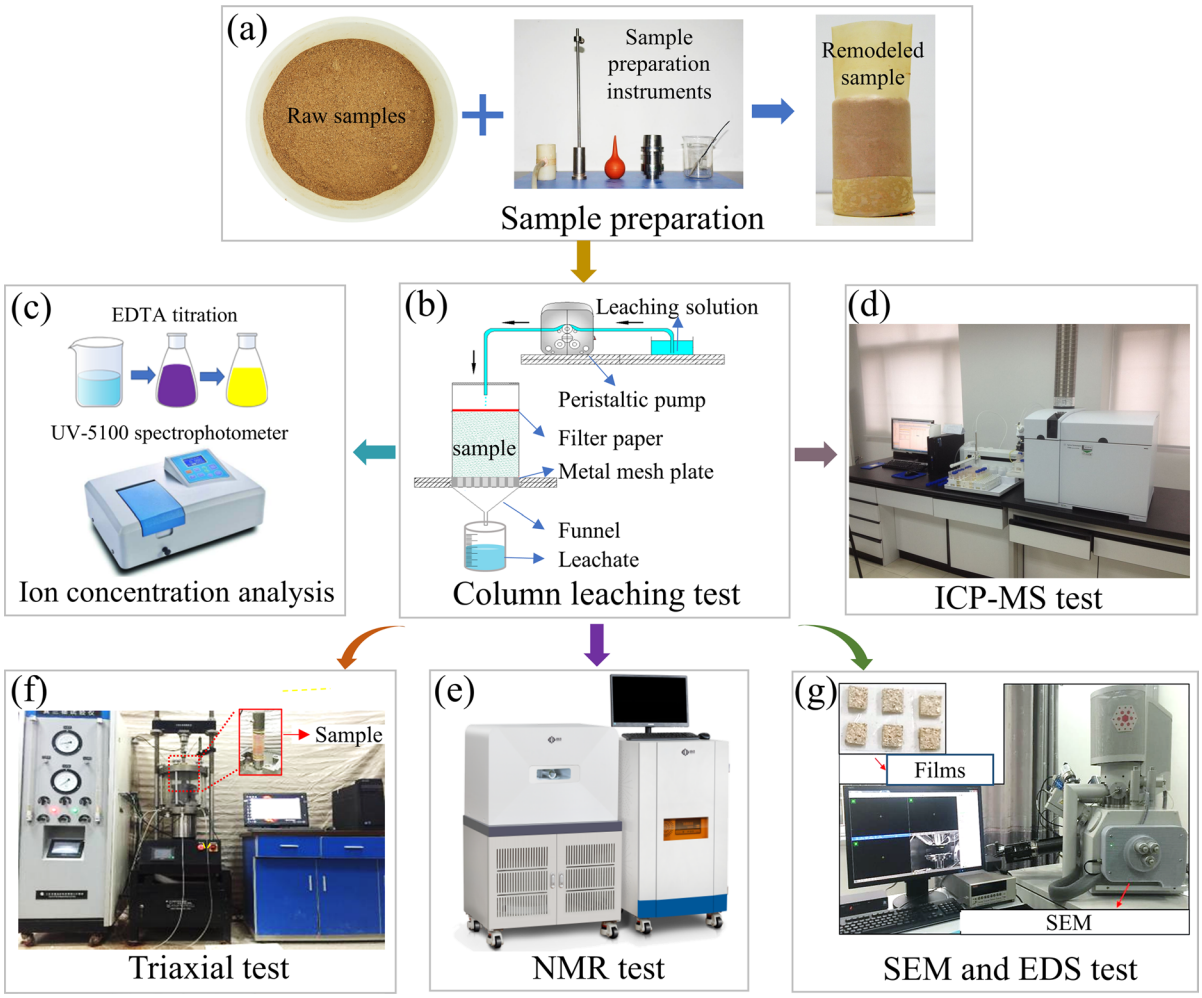

Fig. 2 Schematic diagram of the testing procedure, including sample preparation, column leaching test, ion concentration analysis, ICP-MS test, NMR test, Triaxial test, SEM and EDS test

First, the samples before and after the leaching test were placed in an oven at 60 ℃ for drying; the dried samples were broken off to expose a freshly fractured plane and carefully trimmed to films dimension of 2 cm × 1 cm × 0.5 cm (length × width × height). The films were originally gold-coated by a sputtering machine to increase their conductivity and then fixed onto copper plates. Finally, SEM (XL30W/TMP, Philips) was used to capture images of the coated films. In addition, the chemical composition of the micro-area of the samples was analyzed using EDS. The instrument and sample display are shown in Fig. 2g.

3 Results

3.1 Results of the column leaching test

Figure 3 shows the change in the rare-earth content in the samples and leachate during leaching with 2% $(NH_4)_2SO_4$ solution after 6 h of continuous leaching (12 times in total). After the $(NH_4)_2SO_4$ solution is added, an ion exchange reaction occurs in the sample. NH_4^+ ions displace the RE^{3+} ions adsorbed on the clay surface, accompanied by a declining content of REO in the sample. After 6 times of continuous leaching (3 h later), the leaching solution is continuously injected so that the REO content in the sample

remains unchanged and the NH_4^+ ions concentration is close to the leaching agent concentration. Thus, the main ion exchange reaction occurs in 0–3 h, which is the effective leaching time with the 2% $(NH_4)_2SO_4$ solution under test conditions. According to the residual REO content in the sample and the variation of cations in the leachate, the entire process of column leaching can be divided into two stages: the first one is the main reaction stage (0 h < t ≤ 3 h, ore leaching for 6 times), in which strong ion exchange occurs, and the REO content in the soil drastically decreases along with the leaching of RE^{3+} ions and the consumption of NH_4^+ ions; the second one is the tailing stage (t > 3 h), in which the ion exchange is largely ended, implying that the exchangeable state of rare earths in the sample has been completely exchanged. With the further extension of the leaching time, the REO content in the sample no longer changes, and the rare earth ions in the leachate decrease from the highest concentration, forming a tailing region. It should be noted that the REO content refers to the content of all-phases of rare earths in the specimen, including four phases: (a) water-soluble, (b) ion-exchangeable, (c) colloidal sediment (oxides), (d) mineral (Chi et al. 2005), in which the water-soluble phase are negligible, and conventional electrolyte solutions can extract the ion-exchangeable phase, but not the colloidal sediment phase or the mineral phase (Lai et al. 2018; Moldoveanu and Papangelakis 2012, 2013). In this paper, the final residual REO content in the sample is ~ 176 mg/kg, accounting for ~ 25% of the total REO (shown in Table 2), indicating that the leaching rate of REO is ~ 75%, i.e., the ion-exchanged phase accounted for ~ 75% of the total REO, which is consistent with the results of Chi et al. (Chi et al. 2005).

3.2 Mechanical properties of rare-earth samples during leaching

3.2.1 Stress–strain characteristics of samples

The stress–strain relationship is a crucial mechanical attribute of soil that plays a key role in the study of soil shear behaviors. According to the content of Sect. 3.1, the main reaction stage lasts for 3 h in total. The triaxial compression test was performed to get the stress–strain curves of the sample in the main reaction stage under different confining pressure conditions, as shown in Fig. 4. Under different confining pressures, the stress–strain curves of the sample at different leaching time represent the strain-softening, which are characterized by deviatoric stress peaking along with the increase of strain and declining in the subsequent strain. At the lowest confining pressure tested (50 kPa), the difference between the peak value and residual strength at 15% axial strain

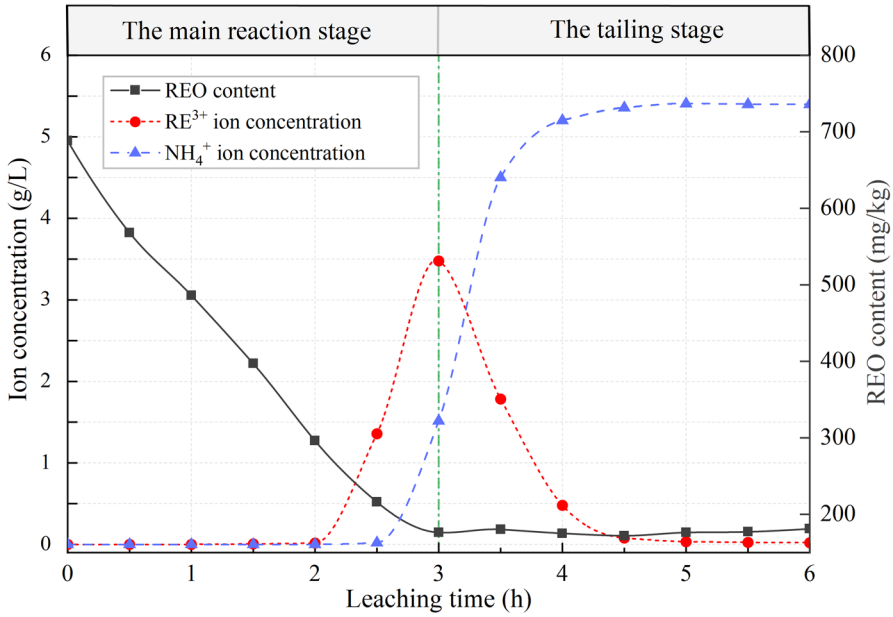

Fig. 3 The change in the rare-earth content in samples and leachate during leaching

is minor, indicating a weak strain-softening behavior. However, the results reveal that increasing the confining pressure leads to a more pronounced softening behavior, as the difference between peak and residual shear strength increases. Hence, higher levels of confining pressure demonstrate a more significant influence on the strain softening behavior. Wang and Li (2022) also characterized a noticeable strain-softening behavior for an intact rare-earth ore subjected to in-situ shear. The observed behavior, attributed to continuous pore water pressure accumulation under undrained conditions reducing effective stress during shearing, results in a significant decrease in shear strength after reaching the peak value (Sadeghi et al. 2019; Nan et al. 2021). Furthermore, this observed strain softening behavior suggests a potential danger of sudden damage with no pre-warning in slopes during leaching processes (Dai et al. 2000; Sadeghi et al. 2019).

Since there is a peak point in the stress–strain curve of each sample, the peak deviatoric stress is considered the shear strength. Figure 5 provides a summary of the shear strength values of samples at different leaching time and confining pressures, indicating that, on the one hand, with the increase of confining pressure at the same leaching stage, e.g., leaching time is 0 h, the shear strength of samples increased from 41.76 kPa to 126.53 kPa, because high confining pressure improved the soil compactness, thus improving the strength (Li et al. 2019; Nan et al. 2021); on the other hand, under the same confining pressure, the shear strength of samples decreases gradually with the leaching time (the main reaction stage). The shear strength of samples decreased by 23.9%, 20.9% and 15.4% for 50 kPa, 100 kPa and 200 kPa confining pressures, respectively; meanwhile, the small decline in the shear strength becomes gradual in the late stage of ore leaching (2–3 h), indicating that the degree of weakening in the shear strength of the rare-earth ore samples diminishes with the end of ore leaching.

The axial strain at the peak state of samples under different confining pressures and leaching time are shown in Fig. 6. Obviously, it is clear that the axial strain increases with the increase of the confining pressure and the leaching time. The axial strain at the peak state at lower confining pressures is smaller than at the peak state at higher confining pressures when the leaching time is the same. This is consistent with the results of (Gu et al. 2019; Nan et al. 2021) who showed that an increase in the confining pressure compacts the soil, resulting in densification of soil particles and filling of soil pores, which in turn increases the axial strain at the peak state. Moreover, at the same confining pressure, the axial strain at the peak

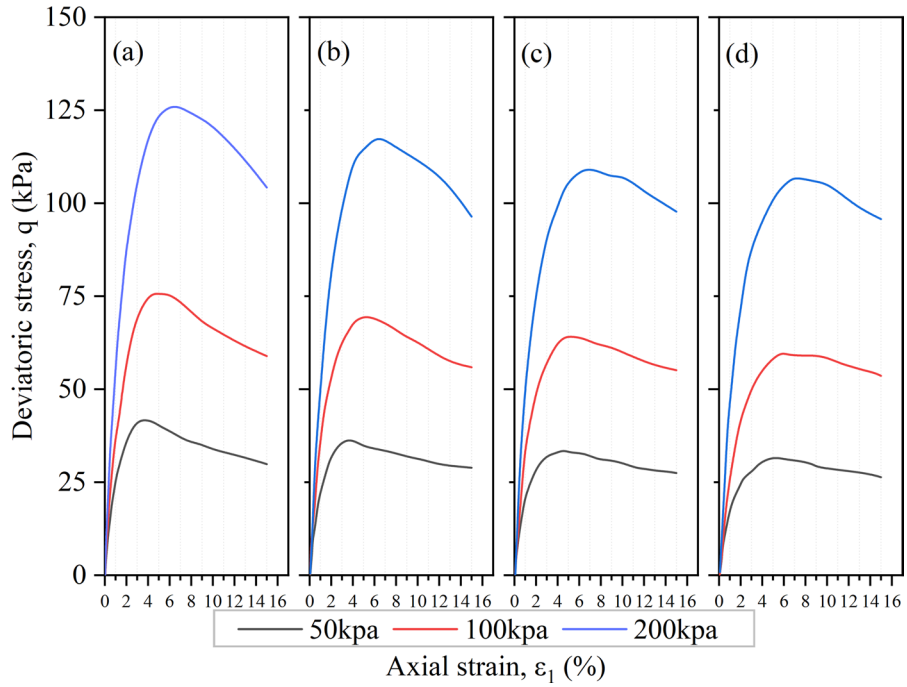

Fig. 4 The change of the stress–strain curve of samples during the leaching process **a**–**d** represent leaching for 0, 1, 2, and 3 h, respectively)

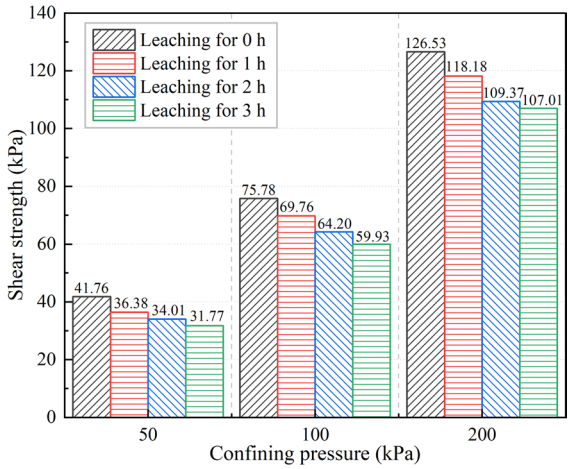

Fig. 5 Shear strength of samples at different leaching time stages

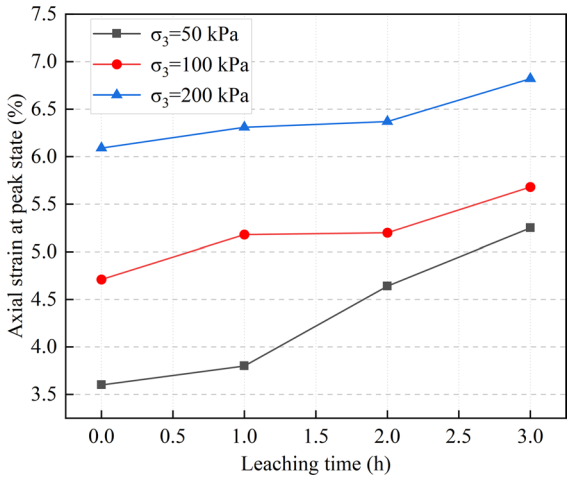

Fig. 6 The axial strain at the peak state of samples under different confining pressures and leaching time

state increases with the leaching time, and the change becomes more distinct under the action of low confining pressures, implying that the pore structure of rare-earth samples has changed due to solution leaching.

3.2.2 Change in the cohesion and internal friction angle of samples

The shear strength parameters of the sample, cohesion (c), and internal friction angle (φ) in the main reaction stage, calculated from the triaxial tests based on the Mohr–Coulomb failure criterion, are shown in Fig. 7. When the leaching time is 0 h, both

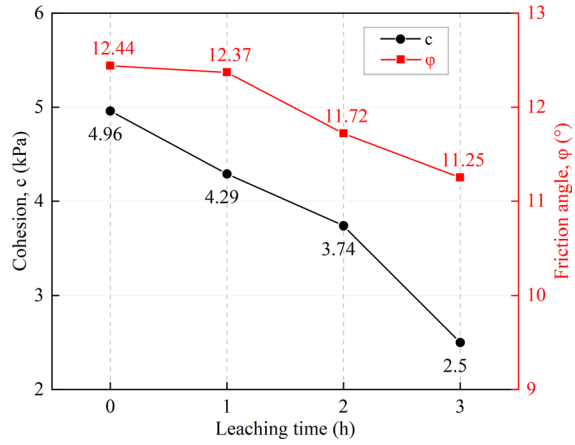

Fig. 7 Relationship between the cohesion and internal friction angle vs. leaching time

c and φ show lower values, which may be related to the saturated water state of the specimen. It is shown by previous researches that water content has a great influence on shear strength parameters (Wang et al. 2016; Gong et al. 2022; Guo et al. 2022). On this basis, the φ of the samples decreases with the leaching time, with a limited change, approximately 9.6%. Similarly, in the main reaction stage, the c decreases from the initial 4.96 to 2.5 kPa, by about 49.6%, along with the increase in leaching time. Similar results were observed in previous studies by conventional triaxial tests or straight shear tests (Huang et al. 2018; Chen et al. 2019).

In conclusion, the shear strength of the specimens is further weakened by the continuous leaching of ammonium sulfate solution, mainly reflected in the decrease of c and φ. These results are consistent with the fact that landslides often occur during in-situ leaching rather than during heavy rainfall (Rao et al. 2016; Chen et al. 2021). However, a further analysis of the microstructural changes in rare-earth samples is required to gain insight into the underlying mechanisms governing the variations in shear strength.

3.3 Microstructural characteristics of the rare-earth samples

3.3.1 T_2 spectrum

In order to reveal the strength weakening mechanism of the orebody in the leaching process, NMR

testing technology was used to test and obtain the T_2 (transverse relaxation time) spectra of samples in the main reaction stage and tailing stage ($0\ \text{h} < t \leq 4$ h, 8 leaching cycles). According to the NMR relaxation mechanism, fluids in different types of pores in soils have different relaxation times, distributed at different positions on the T_2 spectrum. On the one hand, a larger value of relaxation time in the T_2 spectrum reflects a larger pore space in the sample and vice versa. On the other hand, the area enclosed by T_2 spectrum curve and horizontal axis reflects the number of pores in the sample; the larger the enclosed area, the more pores, and vice versa (Li et al. 2020; Du et al. 2022). According to the size of relaxation time in T_2 spectrum, the pores of the sample are divided into three ranges (Li et al. 2020; Zhong et al. 2022): small pore, mesopore and macropore, corresponding to region A ($0 \leq T_2 \leq 10$ ms), region B (relaxation time is $10 < T_2 \leq 100$ ms), region C ($T_2 > 100$ ms) in the T_2 spectrum. Figure 8 shows the T_2 spectrum of samples after eight leaching cycles. The relaxation time T_2 spectrum at 0 h was the initial pore distribution at sample saturation, in which two peaks appear, located in the B and C regions, respectively. When the ammonium sulfate leaching continued until 2.5 h, the peaks of the T_2 spectrum in the B and C regions decreased, and the T_2 spectrum shifted towards the left as a whole, while a third peak appears in the A region. It indicates the evolution of the pores towards small pores, where the proportion of small pores increases and the number of mesopores and macropores decreases. With the continuous leaching of the ore using ammonium sulfate (from 2.5 to 3 h of leaching), the T_2 spectrum shifted to the right overall and showed a rapid decrease in the peak in the A region and an opposite trend in the B and C regions, indicating the pore evolution is characterized by a decrease in the proportion of small pores and an increase in the proportion of mesopore and macropore. The T_2 spectrums of the tailing stage (from 3 to 4 h of leaching) were largely unchanged, implying the pore structure of the samples remained stable after the end of ion exchange.

In addition, NMR technique was used to measure the porosity of the specimens at different leaching times. Since the error of NMR test results was $\pm 1\%$, each test was performed three times to provide an average value of the porosity of the tested samples. The height of the specimens at the end of each leaching cycle was measured to take into account the possibility of swelling or collapse of the soil samples.

Figure 9 shows the changes in porosity and height of the samples during the leaching process It can be observed that the heights of all specimens were unchanged after being leached, indicating that the specimens have not swelled or collapsed. The porosity of the specimens changed with increasing leaching time for different periods: (i) a slow increase of 2.5 from 0 to 2.5 h, (ii) a rapid increase of 2.0 from 2.5 to 3.0 h, and (iii) remained unchanged during

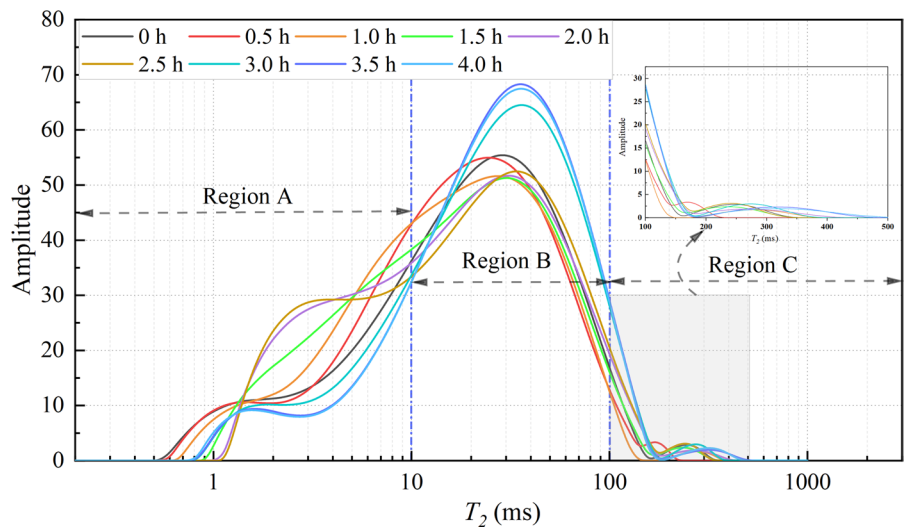

Fig. 8 The T_2 spectrum distribution of samples during the leaching process

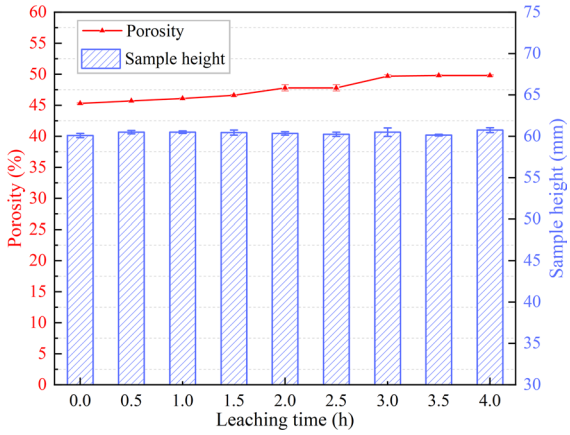

Fig. 9 Changes in sample height and porosity during the leaching process

the tailing phase. The height of the sample remained constant during the leaching process, indicating that the overall skeleton inside the sample did not change significantly. Before being leached with ammonium sulfate, the samples reached a steady state by leaching with DI water for 24 h, so the change in porosity was associated to ion exchange, since almost no new substances or dissolved solid minerals appear during the leaching of ammonium sulfate (Moldoveanu and Papangelakis 2013; Yan et al. 2018; He et al. 2019). In fact, it was observed that the leachate was very turbid during the leaching time of 2.5 to 3 h indicating that the increase in porosity was the result of fine particles migration.

3.3.2 MRI images of samples

MRI images of the specimens were obtained using the NMR analyzer and thus thoroughly characterized the dynamic evolution of the pore structure. As shown in Fig. 10, in the axial direction of the specimen (see coro plane image), the ammonium sulfate leaching causes the overall structure of the specimen to become inhomogeneous, with some black areas (highlighted by yellow circles) appearing and migrating from the upper to the lower part during the main reaction stage (0–3 h of leaching). After 3 h of leaching, the black areas disappeared and the pore structure no longer shows any changes. In general, the leaching process is a top-down reaction between the leaching solution and RE^{3+} ions, and the reaction ends when the ion-exchange reaction front reaches the bottom of the specimen (Xiao 2015). This is because the leaching process conforms to the characteristics of fast extraction kinetics (terminal extraction of a few minutes), is instantaneous compared to the time scale of transport of RE^{3+} ions in the column and is not influenced by the leaching agent concentration (above a threshold related to the ion exchange capacity of the ore) (Stockdale and Banwart 2021), which is also confirmed by the results presented in Fig. 3. The changes in MRI images are synchronous with the ion exchange process in the column leaching test, indicating that the pore structure is strongly influenced by ion exchange. In addition, comparing the MRI images of the leaching time of 0 h and 4 h, it can be observed that the image of Cros1 (near the open surface) becomes brighter than the original one after leaching, while the image of Cros2 (deep into the specimen) shows more black spots, which indicates that more empty voids are formed in the shallow part of the specimen and more dense structures are formed in the deeper part.

3.3.3 SEM and EDS results

Appropriate SEM tests were designed to further observe the changes in the microstructure of ore samples before and after leaching. When the leaching time is 1.5 h, rare-earth samples were extracted from the upper, middle, and lower parts of the ore sample for microscopical observation, and the results are shown in Fig. 11.

Before ammonium sulfate leaching (Fig. 11a and e), the rare-earth sample clearly shows some micrometer-sized elongated fine particles attached to silt particles and coarse particles; When enveloped by elongated fine particles, silt particles are more likely to grow in larger aggregates. Coarse particles and aggregates combine together at the contact surface to form a relatively open soil structure, with obvious macropores in the middle. At 1.5 h of ammonium sulfate leaching, the upper part of the sample shows a more open soil structure, characterized by smaller aggregates and larger pores (Fig. 11b). Meanwhile, the open structure no longer exists in the middle part of the sample, accompanied by an increasing number of fine particles, such as silt particles and aggregates. These fine particles further fill in the pore space

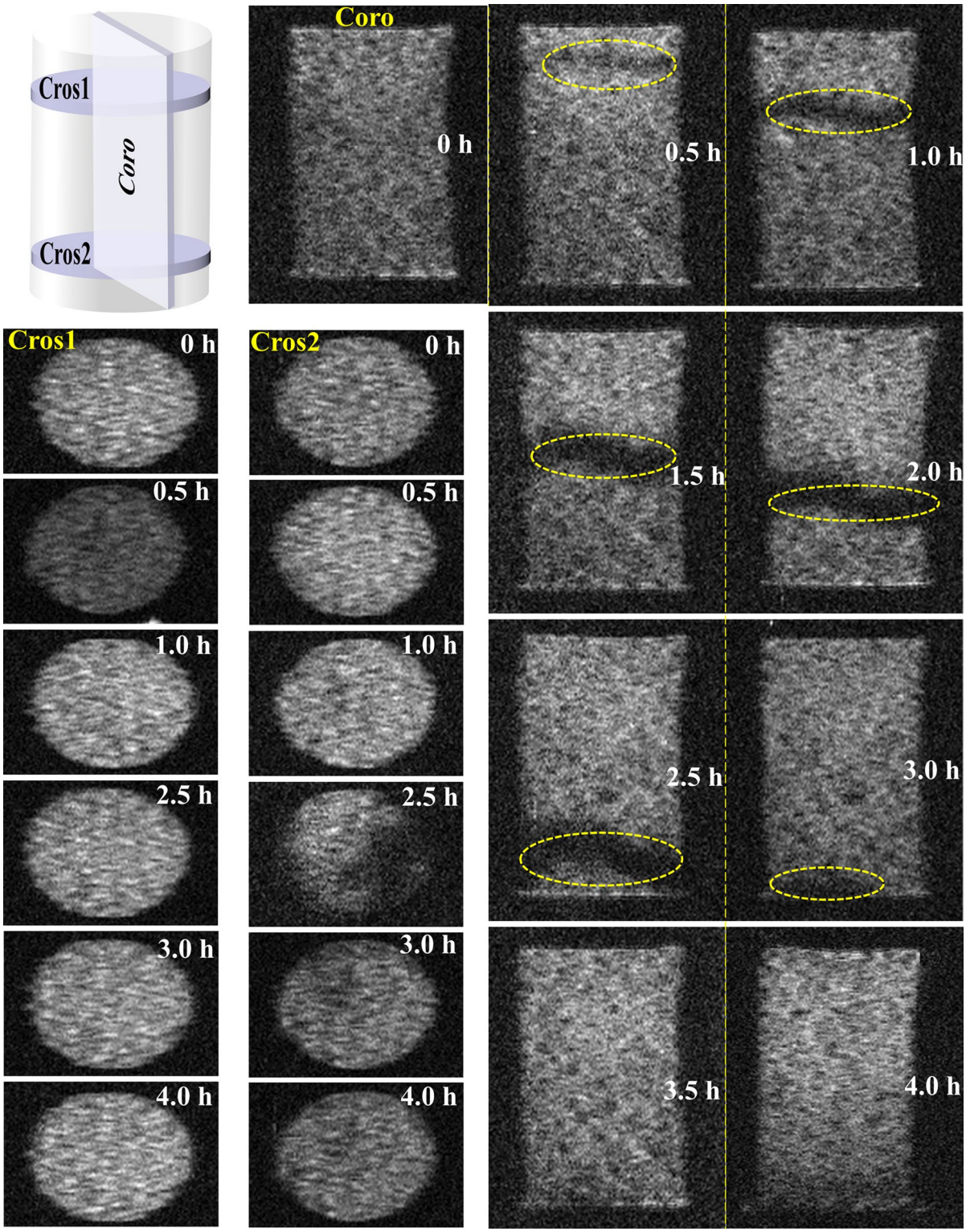

Fig. 10 The MRI images of samples during the leaching process

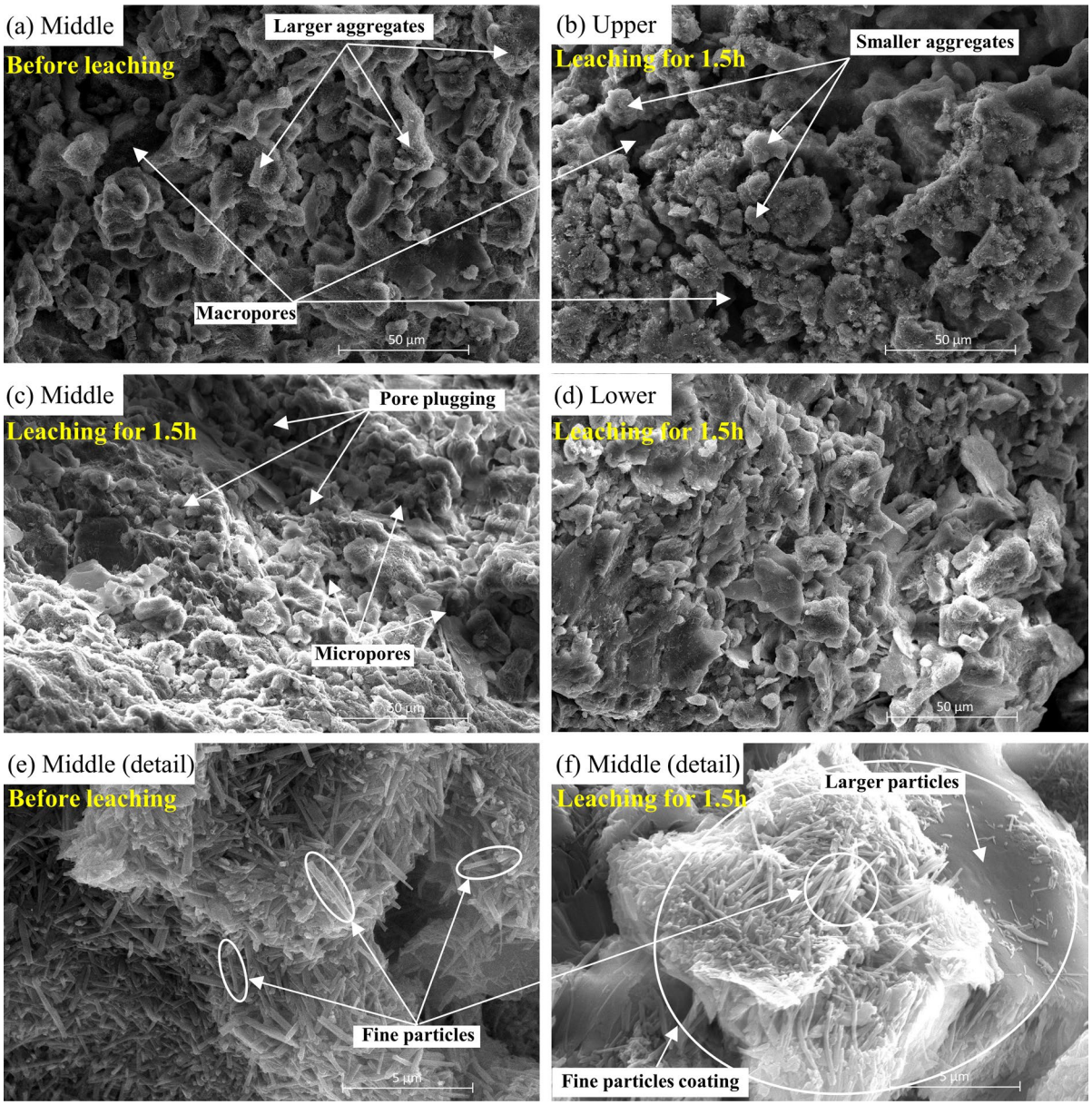

Fig. 11 SEM images of different parts of the sample during the leaching process

between coarse particles or aggregates, thus reducing the pore size (Fig. 11c). The microstructure at the lower part of the sample is similar to that before ammonium sulfate leaching (Fig. 11a and d).

The SEM results demonstrate that these fine particles with characteristics similar to those of clay particles play a crucial role in the reconstruction of pore space. To make a more accurate judgment, EDS was used to analyze the distribution and content of fine particle elements in Fig. 11e and f. The analysis results, as shown in Fig. 12 and Table 4, indicate that the fine particles in Fig. 11e are mainly composed of 11 elements, including O, F, Na, Al, Si, S, K, Ca, Fe, La, and Nd, and the fine particles in Fig. 10f are mainly composed of 7 elements, including N, O, F, Na, Al, Si, and S. At all measuring points, O, Al, and Si account for more than 70% of the sample mass. The SEM images and EDS data perfectly demonstrate

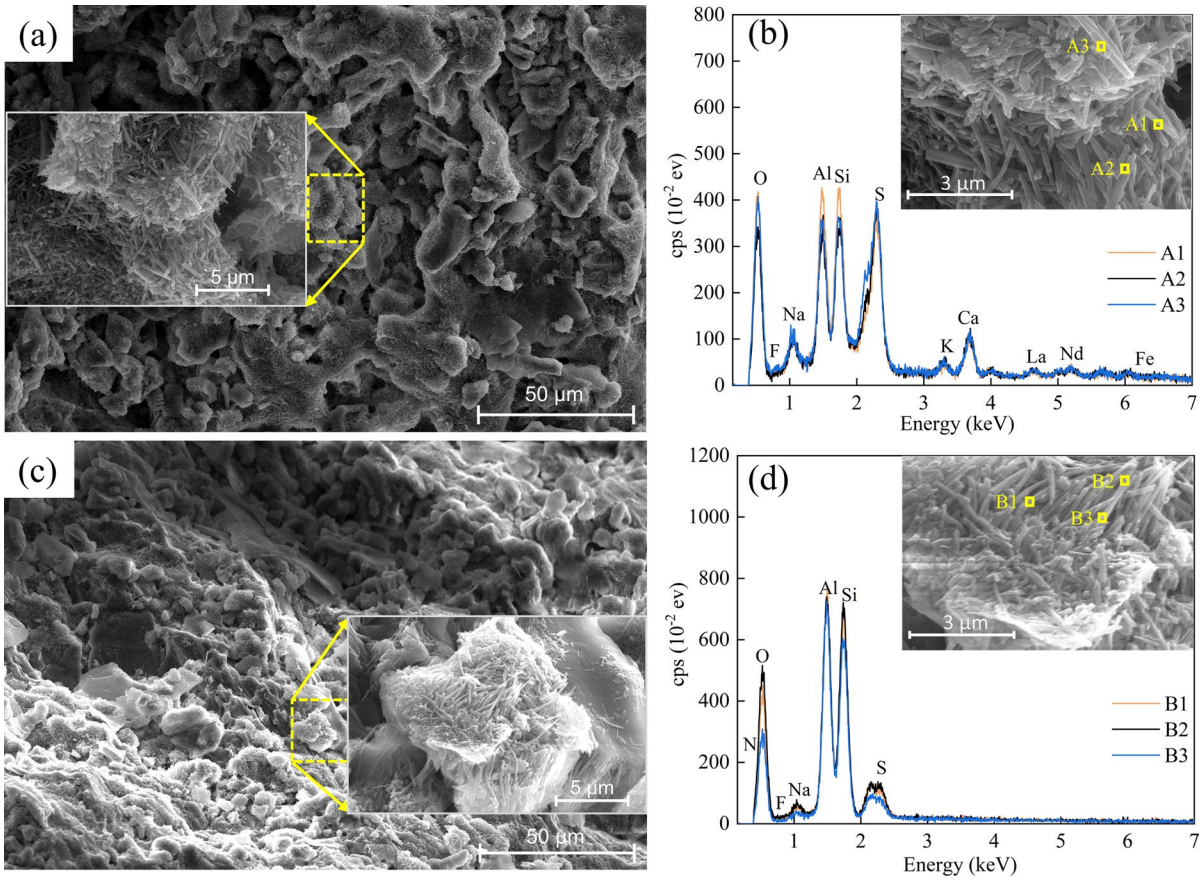

Fig. 12 Layout of the samples areas before and after ammonium sulfate leaching studied by EDS analysis

Table 4 Elemental composition according to the EDS test results (mass fraction %)

Spectrum	Elements											
	N	O	F	Na	Al	Si	S	K	Ca	Fe	La	Nd
A1	–	49.48	0.14	3.97	11.48	10.68	13.86	0.90	3.45	0.11	2.83	3.09
A2	–	54.05	0.41	4.18	10.21	9.35	13.13	1.28	4.28	–	2.24	0.87
A3	–	56.97	–	3.91	11.47	10.23	10.98	1.02	4.10	0.06	0.61	0.64
B1	11.42	52.79	–	1.49	17.14	14.32	2.84	–	–	–	–	–
B2	11.94	53.86	1.48	1.83	14.91	13.17	2.81	–	–	–	–	–
B3	10.66	48.62	–	0.84	20.00	17.26	2.62	–	–	–	–	–

that the fine particle is a typical nanotube-structure halloysite ($Al_2Si_2O_5(OH)_4{\cdot}nH_2O$) (Jing et al. 2017), which is one of the most common clay minerals in rare-earth ores. The loss of Na, K, Ca, Fe, La and Nd elements in the fine particles after leaching can be attributed to ion exchange reactions, as evidenced by the increase in the content of N element.

The results in Sect. 3.3.2 reveals that the ion exchange is completed in the upper part at 1.5 h of leaching. The MRI image of the upper part of (Fig. 10) shows a bright pattern, indicative of a well-developed pore structure. Ion exchange primarily occurs in the middle of the sample, and accordingly, the middle part of the MRI image (Fig. 10) shows a

black area, indicative of a dense pore structure. Furthermore, no ion exchange reaction has occurred in the lower part of the sample, and accordingly, no deviations are found at the lower part of the image. The MRI and SEM images show excellent agreement, demonstrating that at the time of ammonium sulfate leaching, the ion exchange action promotes the dispersion of clay and fine particles in the rare-earth sample in the seepage direction, evidencing certain blockage during the subsequent migration, thereby changing the pore structure.

4 Discussion

The experimental research showed that the rare-earth samples, when saturated and stabilized with DI water and then leached with ammonium sulfate, exhibited a gradually decreasing shear strength (Fig. 5), indicating that the shear strength of undrained rare-earth samples depends on the change in chemical conditions of water inside the pores. Since all prepared samples had almost the same initial density and were sheared under the same stress state, the injected ammonium sulfate solution was the only variable that may have caused the strength variations. The change in the shear behavior, along with the leaching time, is explained in the following part.

The rare-earth sample is composed of coarse particles comprising the soil skeleton, with fine particles filled in the pores between coarse particles, and clay particles enveloping the surface of larger particles as adhesives to form aggregates, generally presenting a relatively open pore space (Fig. 11a). At the time of ammonium sulfate leaching, the solution diffused to soil particles, and NH_4^+ ions in the solution were involved in ion exchange with RE^{3+} ions adsorbed on the mineral surface, resulting in the collapse of the original electrical double layer of soil particles containing high valence counterions and forming a new electric double layer filled with NH_4^+ (monovalent) (Xiao et al. 2018).

The changes caused by the ion exchange process in the electrostatic interaction between soil particles, including electrostatic repulsion, van der Waals attraction, and surface hydration force, could affect the stability of soil aggregates (Ding et al. 2019a; Muneer et al. 2022). In this regard, the research conducted by Ding et al. (2019b) showed that the stability of soil aggregates is intensely affected by the type and concentration of electrolyte, consequently depending on the electrostatic interaction between soil particles. In addition, they concluded that the cationic valence plays a much more important role than the concentration in maintaining the stability of soil aggregates, i.e. a critical electrolyte concentration of 0.005 mol/L for divalent Mg^{2+} soils and 0.25 mol/L for monovalent Na^+ soils. For the investigated rare-earth samples, the stability of soil aggregates before ammonium sulfate leaching was attributed to its trivalent RE^{3+} ions, although the ions remain at a low concentration. When ammonium sulfate was used for leaching (0–2.5 h), the decreased effective cationic valence on soil particles led to the depolymerization of soil aggregates, as shown in Fig. 11b. It can be observed that smaller fine particles were separated from coarse particles and that the dispersion of fine particles and subsequent blockage caused the soil's overall pore size transforms from macropores and mesopores to micropores (Fig. 8). When the leaching time reached 3 h, ion exchange was completed at the lower part of the sample, and the pore distribution started to transform from small pores to larger ones, which is attributed to some fine particles flowing out of the sample at the end of ion exchange. Similar release and deposition behavior of in situ particles from soils has been observed in other studies associated with dynamic changes in soil pore water chemistry conditions (Roy and Dzombak 1996; Grolimund and Borkovec 2006; Bradford and Kim 2010; Tan et al. 2022). In this study, the mobilization behavior of fine particles was coupled with changes in ion exchange fronts, and Fig. 13 vividly demonstrates the evolution of pore structure of rare-earth samples.

It should be noted that the specimens in this paper did not collapse due to particle migration, and their total volume remained unchanged (Fig. 9), which is generally denoted as suffusion (Prasomsri and Takahashi 2020). In this study, the top-down migration of fine particles under the action of ion exchange and seepage changes the original uniformity of the soil, gradually forming a structure with a loose upper part and a dense lower part (Fig. 13). Previous studies showed that the overall shear strength of such inhomogeneous soils was more prone to the formation of local parts with weaker bearing capacity, for example, failure first occurs in the parts with larger porosity (Hu et al. 2018; Zheng et al. 2019a,b). In the long run,

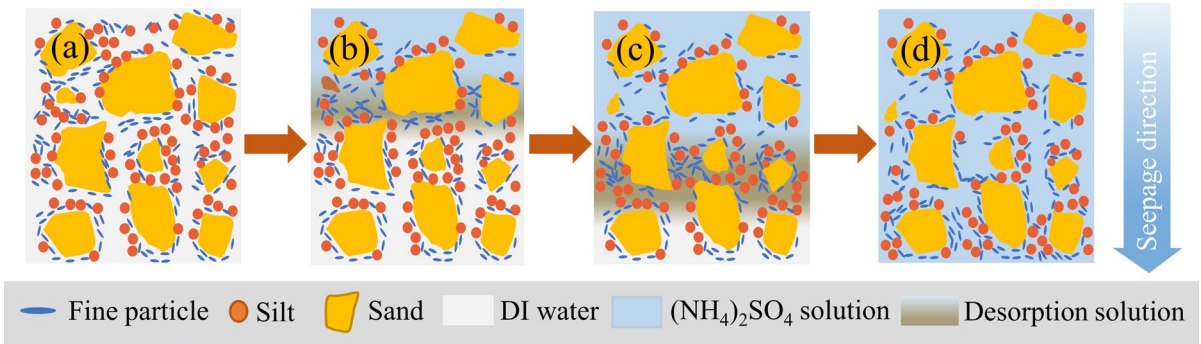

Fig. 13 The structural change of the sample during ammonium sulfate leaching

as the leaching proceeds, the continual loss of fine particles in the upper part of the sample results in the formation of larger macropores and a coarser matrix support structure characterized by higher compressibility and lower shear strength (Fan et al. 2017; Lei et al. 2020). This is demonstrated by the fact that the axial strain at peak stress on the stress–strain curve increases with the leaching time, while the shear strength progressively lowers. Furthermore, the effect of leaching on shear strength is mainly reflected in the reduction of cohesion, which is due to the loss of fine particles resulting in weaker electrostatic attraction between soil particles; followed by a small reduction in the angle of internal friction, probably because the interlocking structure between the large particles did not change significantly.

In conclusion, the particle migration caused by ion exchange and seepage during the leaching process of RE^{3+} ions from ore is an important factor that aggravates the degradation of the soil structure of rare-earth ores, further threatening the stability of the ore slope. As a result, to avoid or alleviate fatal consequences caused by ore leaching, future development is related to finding novel leaching agents to prevent particle migration or to the optimization of existing leaching methods (Zhang et al. 2021; Muneer et al. 2022; Wang et al. 2023). It is also important to note that the experiment was conducted under controlled laboratory conditions. Due to external interfering factors in the physical and chemical process and the engineering geological characteristics of the ore body itself, the ore body slope at the site may exhibit different stability results (Wei et al. 2023). In addition, the increased pore water pressure and water content caused by local particle blockage also significantly contribute to an increased number of landslide events, which can occur simultaneously with the degradation of soil structure (Hu et al. 2017, 2018; Lei et al. 2017). The decrease in permeability caused by ammonium sulfate leaching has been confirmed by previous studies. Therefore, long-term monitoring of the ore body's pore water pressure can be an effective early warning measure for risk management.

5 Conclusions

(1) Under the test conditions, when the effective leaching time with 2% ammonium sulfate is 0–3 h, which is a period defined as the main reaction stage, the sample exhibits a decreased peak strength, accompanied by reduced cohesion (c) and internal friction angle (φ), and a large axial strain at peak stress, with the leaching time.
(2) In the main reaction stage, the top-down ion exchange in the sample results in the dispersion and migration of fine particles in the ore samples in the seepage direction, leading to the re-development of the pore structure in the sample. In the early stage of ore leaching, the pore structure mainly evolves from medium and macropores to small pores, and in the later stage, the sample begins to demonstrate a decreased number of micropores and an increased number of medium pores and macropores.
(3) In the main reaction stage, the top-down migration process of fine particles in the rare-earth sample results in an unstable structure of the soil, characterized by a loose upper part, a dense lower

part and an overall greater porosity. This weakens the bonding strength and interlocking effect between particles, which, on the macroscopic level, leads to a decreasing the shear strength parameters of the rare-earth sample.

Author contribution HW: Conceptualization, methodology, writing—original draft. XW: Supervision, funding acquisition, writing—review & editing. GL: Data curation, validation. HY: Formal analysis, investigation. CZ: Visualization, software. LZ: Project administration, formal analysis, visualization.

Funding This research was supported by the National Natural Science Foundation of China (Grant Nos. 52174113, 51874148), the Young Jinggang Scholars Award Program in Jiangxi Province (QNJG2018051) and the "Thousand Talents" of Jiangxi Province (jxsq2019201043).

Data availability Some or all data, models, or codes generated or used during the study are available from the corresponding author by request.

Declarations

Ethics approval Not applicable.

Consent to publish All authors of this article consent to publish.

Competing interests The authors declare no competing interests.

References

Aiban SA, Al-Ahmadi HM, Asi IM et al (2006) Effect of geotextile and cement on the performance of sabkha subgrade. Build Environ 41:807–820. https://doi.org/10.1016/j.buildenv.2005.03.006

Bai W, Zhang W, Kong L et al (2023) Effect of soaking time of dithionite e citrate e bicarbonate solution on strength and deformation characteristics of lateritic soil. J Rock Mech Geotech Eng. https://doi.org/10.1016/j.jrmge.2023.02.003

Borst AM, Smith MP, Finch AA et al (2020) Adsorption of rare earth elements in regolith-hosted clay deposits. Nat Commun 11:1–15. https://doi.org/10.1038/s41467-020-17801-5

Bradford SA, Kim H (2010) Implications of cation exchange on clay release and colloid-facilitated fransport in porous media. J Environ Qual 39:2040–2046. https://doi.org/10.2134/jeq2010.0156

Chen R, Fu H, Yong S et al (2021) Characteristics and genetic analysis of landslide in rare earth leaching mining area. Jiangxi Build Mater 264:183–185

Chen X, Qi Y, Yin SH et al (2019) Law of weakening mechanical properties of rare earth ore with leaching. J Central South Univ Sci Technol 50:939–945. https://doi.org/10.11817/j.issn.1672-7207.2019.04.023

Chen Z, Zhang Z, Liu D et al (2020) Swelling of clay minerals during the leaching process of weathered crust elution-deposited rare earth ores by magnesium salts. Powder Technol 367:889–900. https://doi.org/10.1016/j.powtec.2020.04.008

Chi R, Tian J, Li Z et al (2005) Existing state and partitioning of rare earth on weathered ores. J Rare Earths 23:756–759

Chitravel S, Otsubo M, Kuwano R (2021) Experimental study on stiffness degradation and monotonic response of reconstituted volcanic ash induced by internal erosion. Soils Found 61:1431–1452. https://doi.org/10.1016/j.sandf.2021.08.003

Dai FC, Chen SY, Lee CF (2000) Analysis of landslide initiative mechanism based on stress-strain behaviour of soil. Chin J Geotech Eng 22:127–130

Deng Z, Qin L, Wang G et al (2019) Metallogenic process of ion adsorption REE ore based on the occurrence regularity of La in kaolin. Ore Geol Rev 112:103022. https://doi.org/10.1016/j.oregeorev.2019.103022

Ding W, Liu X, Hu F et al (2019a) How the particle interaction forces determine soil water infiltration: Specific ion effects. J Hydrol 568:492–500. https://doi.org/10.1016/j.jhydrol.2018.11.017

Ding W, Liu X, Hu F et al (2019b) The effect of interactions between particles on soil infiltrability. J Soils Sediments 19:3489–3498. https://doi.org/10.1007/s11368-019-02318-2

Du C, Bi J, Zhao Y, Wang C (2022) A stratified NMR-Based investigation of spatial evolution of pore structure in sandstone after cyclic heating and local water cooling. Nat Resour Res 31:3365–3392. https://doi.org/10.1007/s11053-022-10123-x

Dushyantha N, Batapola N, Ilankoon IMSK et al (2020) The story of rare earth elements (REEs): occurrences, global distribution, genesis, geology, mineralogy and global production. Ore Geol Rev 122:103521. https://doi.org/10.1016/j.oregeorev.2020.103521

Fan X, Xu Q, Scaringi G et al (2017) A chemo-mechanical insight into the failure mechanism of frequently occurred landslides in the Loess Plateau, Gansu

Province, China. Eng Geol 228:337–345. https://doi.org/10.1016/j.enggeo.2017.09.003

Fu W, Luo P, Hu Z et al (2019) Enrichment of ion-exchangeable rare earth elements by felsic volcanic rock weathering in South China: Genetic mechanism and formation preference. Ore Geol Rev 114:103120. https://doi.org/10.1016/j.oregeorev.2019.103120

GB/T 50123–2019 (2019) Standard for Geotechnical Testing Method. China Planning Press, Beijing, China

Gong W, Quan C, Li X et al (2022) Statistical analysis on the relationship between shear strength and water saturation of cohesive soils. Bull Eng Geol Env 81:337. https://doi.org/10.1007/s10064-022-02811-y

Gratchev I, Towhata I (2013) Stress–strain characteristics of two natural soils subjected to long-term acidic contamination. Soils Found 53:469–476. https://doi.org/10.1016/j.sandf.2013.04.008

Grolimund D, Borkovec M (2006) Release of colloidal particles in natural porous media by monovalent and divalent cations. J Contam Hydrol 87:155–175. https://doi.org/10.1016/j.jconhyd.2006.05.002

Gu T, Wang J, Wang C et al (2019) Experimental study of the shear strength of soil from the Heifangtai Platform of the Loess Plateau of China. J Soils Sediments 19:3463–3475. https://doi.org/10.1007/s11368-019-02303-9

Guo Z, Zhou J, Xu H et al (2022) Reviews of ionic type rare earth orebody strength weakening and landslide under ore leaching. Chin Rare Earths 43:9–22. https://doi.org/10.16533/J.CNKI.15-1099/TF.20220044

Guo Z, Zhou J, Zhou K et al (2021) Soil-water characteristics of weathered crust elution-deposited rare earth ores. Trans Nonferrous Met Soc China 31:1452–1464. https://doi.org/10.1016/S1003-6326(21)65589-9

He Z, Zhang R, Nie W et al (2019) Leaching process and mechanism of weathered crust elution-deposited rare earth ore. Min Metall Explor 36:1021–1031. https://doi.org/10.1007/s42461-019-00116-5

Hong B, Luo S, Hu S et al (2019) Influence of matric suction on shear strength of unsaturated ion-absorbed rare earth. Yantu Lixue/rock Soil Mech 40:2303–2310. https://doi.org/10.16285/j.rsm.2018.0352

Hu W, Hicher PY, Scaringi G et al (2018) Seismic precursor to instability induced by internal erosion in loose granular slopes. Geotechnique 68:989–1001. https://doi.org/10.1680/jgeot.17.P.079

Hu W, Scaringi G, Xu Q et al (2017) Sensitivity of the initiation and runout of flowslides in loose granular deposits to the content of small particles: An insight from flume tests. Eng Geol 231:34–44. https://doi.org/10.1016/j.enggeo.2017.10.001

Huang G, Zhuo Y, Wang X et al (2018) Effects of different concentration in leaching liquid on rare earth ore's strength. Chin Rare Earths 39:47–54. https://doi.org/10.16533/J.CNKI.15-1099/TF.201803007

Huang XW, Long ZQ, Wang LS, Feng ZY (2015) Technology development for rare earth cleaner hydrometallurgy in China. Rare Met 34:215–222. https://doi.org/10.1007/s12598-015-0473-x

Jing Q, Chai L, Huang X et al (2017) Behavior of ammonium adsorption by clay mineral halloysite. Trans Nonferrous Met Soc China 27:1627–1635. https://doi.org/10.1016/S1003-6326(17)60185-7

Lai FG, Huang L, Gao GH et al (2018) Recovery of rare earths from ion-absorbed rare earths ore with $MgSO_4$-ascorbic acid compound leaching agent. J Rare Earths 36:521–527. https://doi.org/10.1016/j.jre.2017.12.003

Lei H, Wang L, Jia R et al (2020) Effects of chemical conditions on the engineering properties and microscopic characteristics of Tianjin dredged fill. Eng Geol 269:105548. https://doi.org/10.1016/j.enggeo.2020.105548

Lei X, Yang Z, He S et al (2017) Numerical investigation of rainfall-induced fines migration and its influences on slope stability. Acta Geotech 12:1431–1446. https://doi.org/10.1007/s11440-017-0600-y

Li M, Wang D, Shao Z (2020) Experimental study on changes of pore structure and mechanical properties of sandstone after high-temperature treatment using nuclear magnetic resonance. Eng Geol 275:105739. https://doi.org/10.1016/j.enggeo.2020.105739

Li P, Xie W, Pak RYS, Vanapalli SK (2019) Microstructural evolution of loess soils from the Loess Plateau of China. CATENA 173:276–288. https://doi.org/10.1016/j.catena.2018.10.006

Liu D, Zhang Z, Chi R et al (2020a) Experimental study on the influence of particle size on the strength characteristics of weathered crust elution-deposited rare earth ores. Nonferrous Met Eng 10:97–103. https://doi.org/10.3969/j.issn.2095-1744.2020.06.015

Liu D, Zhang Z, Chi R (2020b) Seepage mechanism during in-situ leaching process of weathered crust elution-deposited rare earth ores with magnesium salt. Physicochem Probl Min Process 56:350–362. https://doi.org/10.37190/ppmp/117925

Luo X, Zhang Y, Zhou H et al (2022) Pore structure characterization and seepage analysis of ionic rare earth orebodies based on computed tomography images. Int J Min Sci Technol 32:411–421. https://doi.org/10.1016/j.ijmst.2022.02.006

Moldoveanu GA, Papangelakis VG (2012) Recovery of rare earth elements adsorbed on clay minerals: I. Desorption Mechanism. Hydrometallurgy 117–118:71–78. https://doi.org/10.1016/j.hydromet.2012.02.007

Moldoveanu GA, Papangelakis VG (2013) Recovery of rare earth elements adsorbed on clay minerals: II. Leaching with Ammonium Sulfate. Hydrometallurgy 131–132:158–166. https://doi.org/10.1016/j.hydromet.2012.10.011

Muneer R, Hashmet MR, Pourafshary P (2022) Predicting the critical salt concentrations of monovalent and divalent brines to initiate fines migration using DLVO modeling. J Mol Liq 352:118690. https://doi.org/10.1016/j.molliq.2022.118690

Nan J, Peng J, Zhu F et al (2021) Shear behavior and microstructural variation in loess from the Yan'an area, China. Eng Geol 280:105964. https://doi.org/10.1016/j.enggeo.2020.105964

Nie W, Zhang R, He Z et al (2020) Research progress on leaching technology and theory of weathered crust elution-deposited rare earth ore. Hydrometallurgy 193:105295. https://doi.org/10.1016/j.hydromet.2020.105295

Peng H, Hu S, Wang G et al (2022) The influence of leaching agent concentration on the shear strength parameters of ion-adsorption rare earth ore. Chin Rare Earths

43:58–64. https://doi.org/10.16533/j.cnki.15-1099/tf.20220056

Peng K, Peng H, Liang F et al (2017) Distribution characteristics and development environment of geological disasters in Ganzhou City. Saf Environ Eng 24:33–39. https://doi.org/10.13578/j.cnki.issn.1671-1556.2017.01.006

Prasomsri J, Takahashi A (2020) The role of fines on internal instability and its impact on undrained mechanical response of gap-graded soils. Soils Found 60:1468–1488. https://doi.org/10.1016/j.sandf.2020.09.008

Rao R, Li M, Zhang S et al (2016) Experimental study on landslide features and countermeasures of in-situ leaching stope of ion-type rare earth mines. Chin Rare Earths 37:26–31. https://doi.org/10.16533/J.CNKI.15-1099/TF.201606005

Roy SB, Dzombak DA (1996) Na^{+}–Ca^{2+} exchange effects in the detachment of latex colloids deposited in glass bead porous media. Colloids Surf A Physicochem Eng Asp 119:133–139. https://doi.org/10.1016/S0927-7757(96)03764-8

Sadeghi H, Kiani M, Sadeghi M, Jafarzadeh F (2019) Geotechnical characterization and collapsibility of a natural dispersive loess. Eng Geol 250:89–100. https://doi.org/10.1016/j.enggeo.2019.01.015

Salgado R, Bandini P, Karim A (2000) Shear strength and stiffness of silty sand. J Geotech Geoenviron Eng 126:451–462

Stockdale A, Banwart SA (2021) Recovery of technologically critical lanthanides from ion adsorption soils. Miner Eng 168:106921. https://doi.org/10.1016/j.mineng.2021.106921

Tan B, Liu C, Tan X et al (2022) Heavy metal transport driven by seawater-freshwater interface dynamics: The role of colloid mobilization and aquifer pore structure change. Water Res 217:118370. https://doi.org/10.1016/j.watres.2022.118370

Tang X, Li M, Yang D (2000) Stope slide in in-situ leaching of ionic type rare-earch ore and its countermeasures. Met Mine 289:6–8+12

Tian J, Chi R, Yin J (2010) Leaching process of rare earths from weathered crust elution-deposited rare earth ore. Trans Nonferrous Met Soc China 20:892–896. https://doi.org/10.1016/S1003-6326(09)60232-6

Wang D, Li J (2022) Analysis of mechanical properties of rare earth ore-body based on in-situ shear experiment. Chin Rare Earths 43:75–81. https://doi.org/10.16533/j.cnki.15-1099/tf.20220018

Wang G, Luo S, Hu S et al (2017) Seepage process and slope deformation of barefoot type rare earth mine in-situ leaching. Chin Rare Earths 38:35–46. https://doi.org/10.16533/J.CNKI.15-1099/TF.201703005

Wang G, Xu J, Ran L et al (2023) A green and efficient technology to recover rare earth elements from weathering crusts. Nat Sustain 6:81–92. https://doi.org/10.1038/s41893-022-00989-3

Wang H, Qiu G, Luo T (2016) Effect of saturation degree on shear strength of ion-adsorption rare-earth ore. China Min Mag 25:460–464

Wang X, Wang H, Sui C et al (2020) Permeability and adsorption–desorption behavior of rare earth in laboratory leaching tests. Minerals 10:889. https://doi.org/10.3390/min10100889

Wei L, Xu Q, Wang S, Ji X (2023) The primary influence of shear band evolution on the slope bearing capacity. J Rock Mech Geotech Eng. https://doi.org/10.1016/j.jrmge.2022.12.021

Xiao T, Li P, Shao S (2022) Fractal dimension and its variation of intact and compacted loess. Powder Technol 395:476–490. https://doi.org/10.1016/j.powtec.2021.09.069

Xiao Y (2015) Study on the green and efficient leaching technology for ion-adsorption type rare earths ore with magnesium salt system. Northeastern University, Boston

Xiao Y, Gao G, Huang L et al (2018) A discussion on the leaching process of the ion-adsorption type rare earth ore with the electrical double layer model. Miner Eng 120:35–43. https://doi.org/10.1016/j.mineng.2018.02.015

Xu P, Zhang Q, Qian H et al (2021) Exploring the geochemical mechanism for the saturated permeability change of remolded loess. Eng Geol 284:105927. https://doi.org/10.1016/j.enggeo.2020.105927

Yan H, Liang T, Liu Q et al (2018) Compound leaching behavior and regularity of ionic rare earth ore. Powder Technol 333:106–114. https://doi.org/10.1016/j.powtec.2018.04.010

Yang L, Wang D, Li C et al (2018) Searching for a high efficiency and environmental benign reagent to leach ion-adsorption rare earths based on the zeta potential of clay particles. Green Chem 20:4528–4536. https://doi.org/10.1039/c8gc01569d

Yang M, Liang X, Ma L et al (2019) Adsorption of REEs on kaolinite and halloysite: a link to the REE distribution on clays in the weathering crust of granite. Chem Geol 525:210–217. https://doi.org/10.1016/j.chemgeo.2019.07.024

Yang SQ, Xu SB, Liu Z et al (2023) Experimental investigation on the triaxial unloading mechanical characteristics of sandstone immersed in different brines. Geomech Geophys Geo-Energy Geo-Resour 9:71. https://doi.org/10.1007/s40948-023-00602-7

Yang XJ, Lin A, Li XL et al (2013) China's ion-adsorption rare earth resources, mining consequences and preservation. Environ Dev 8:131–136. https://doi.org/10.1016/j.envdev.2013.03.006

Yin S, Chen X, Yan R, Wang L (2021) Pore structure characterization of undisturbed weathered crust elution-deposited rare earth ore based on X-ray micro-CT scanning. Minerals 11:236. https://doi.org/10.3390/min11030236

Yin S, Qi Y, Xie F et al (2018) Strength characteristics of weathered crust elution-deposited rare earthores with different porosity ratios. Chin J Eng 40:159–166. https://doi.org/10.13374/j.issn2095-9389.2018.02.005

Yuan W, Fan W (2022) Quantitative study on the microstructure of loess soils at micrometer scale via X-ray computed tomography. Powder Technol 408:117712. https://doi.org/10.1016/j.powtec.2022.117712

Zhang P, Tao K, Yang Z (1995) Study on material composition and REE-host forms of Ion-type RE deposits in South China. J Rare Earths 13:37–41

Zhang Y, Zhang B, Yang S et al (2021) Enhancing the leaching effect of an ion-absorbed rare earth ore by ameliorating the seepage effect with sodium dodecyl sulfate surfactant. Int J Min Sci Technol 31:995–1002. https://doi.org/10.1016/j.ijmst.2021.06.002

Zhang Z, He Z, Yu J et al (2016) Novel solution injection technology for in-situ leaching of weathered crust elution-deposited rare earth ores. Hydrometallurgy 164:248–256. https://doi.org/10.1016/j.hydromet.2016.06.015

Zheng H, Wang D, Behringer RP (2019a) Experimental study on granular biaxial test based on photoelastic technique. Eng Geol 260:105208. https://doi.org/10.1016/j.enggeo.2019.105208

Zheng H, Wang D, Tong X et al (2019b) Granular scale responses in the shear band region. Granul Matter 21:1–6. https://doi.org/10.1007/s10035-019-0958-7

Zhong W, Ouyang J, Yang D et al (2022) Effect of the in situ leaching solution of ion-absorbed rare earth on the mechanical behavior of basement rock. J Rock Mech Geotech Eng 14:1210–1220. https://doi.org/10.1016/j.jrmge.2021.12.002

Zhou L, Wang X, Huang C et al (2021) Development of pore structure characteristics of a weathered crust elution-deposited rare earth ore during leaching with different valence cations. Hydrometallurgy 201:105579. https://doi.org/10.1016/j.hydromet.2021.105579